



Trans. Nonferrous Met. Soc. China 33(2023) 563-575

Transactions of Nonferrous Metals Society of China

www.tnmsc.cn



Mechanism and kinetics for chlorination roasting of copper smelting slag

Bei-kai ZHANG^{1,2}, Qin-meng WANG^{1,2}, Xue-yi GUO^{1,2}, Qing-hua TIAN^{1,2}

- 1. School of Metallurgy and Environment, Central South University, Changsha 410083, China;
- National & Regional Joint Engineering Research Center of Nonferrous Metal Resource Recycling, Changsha 410083, China

Received 9 November 2021; accepted 30 March 2022

Abstract: An efficient process based on chlorination roasting with CaCl₂ was proposed to recover zinc from copper smelting slag. The reaction mechanism and the kinetics of the chlorination process were investigated by thermodynamic calculation, thermogravimetry and differential scanning calorimetry (TG-DSC) analysis and X-ray diffraction (XRD) methods. The results demonstrated that the temperatures of oxidative decomposition of CaCl₂ and chlorination of all Zn-containing phases were above 774.3 and 825 °C, respectively. The chlorination roasting process was divided into four stages: precipitation of adsorbed water, extraction of crystallized water, oxidation of Fe-containing phases, and chlorination volatilization of zinc. The average apparent activation energies of the iron oxidation and zinc chlorination were 101.70 and 84.4 kJ/mol, respectively. The most probable mechanism function for the iron oxidation process was the Avrami–Erofeev model (*n*=2). Zinc chlorination followed the shrinking unreacted core model, and the chemical reaction was the rate-controlling step.

Key words: copper smelting slag; chlorination roasting; CaCl₂; thermodynamics; kinetics; iron; zinc

1 Introduction

Copper is a strategic raw material widely used in the defense industry and new technological revolution [1]. At present, more than 95% of refined copper in China is produced by the pyrometallurgical process, which produce a large amount of copper smelting slag [2]. Copper smelting slag is a typical secondary resource of nonferrous metals, containing large amounts of valuable components (e.g., Cu, Zn and Pb) with great recycling value [3]. However, it is difficult to recover the valuable components from copper smelting slag by traditional metallurgical processes because of its stable structure and complicated multi-component system [4].

Generally, slow-cooling flotation is the primary method for recovering copper from copper

smelting slags, which is widely used in copper pyrometallurgy [5]. Flotation technology can efficiently recover copper with low energy consumption; however, other components in the copper smelting slag cannot be recycled. At present, many studies have been focused on comprehensive utilization of copper smelting slags. ZHANG et al [6] proposed alkali disaggregation of fayalite coupled with an acid leaching process to extract valuable metals from copper smelting slag; the total leaching efficiencies of As, Zn, Fe, Cu, and Pb were 99.7%, 62.5%, 41.5%, 99.9%, and 99.1%, respectively, in the HNO₃-H₂O₂ system. WAN et al [7] investigated the recovery of Co, Ni, and Cu from copper smelting slag by utilizing waste SO₂ gas and residual heat. The results showed that the recovery efficiencies of Ni, Co, and Cu were 95.8%, 91.8%, and 81.6%, respectively, under optimized sulfation roasting conditions followed by water leaching. ZULHAN et al [8] proposed a production process for ferro-silicon-manganese from a mixture of manganese ore and copper smelting slag at a temperature above 1450 °C. Although the above recycling methods have better recovery effects, the recovery processes are complex and require harsh operating conditions. Thus, a simple and efficient method to recover valuable metals from copper smelting slags is necessary.

Chlorination roasting can effectively separate valuable metals from metallurgical solid waste, which has a stable structure and complicated multi-component system [9]. Based on the different properties of the raw materials and subsequent treatment methods, the chlorination metallurgy method can be divided into high-temperature and moderate-temperature chlorination roasting. The high-temperature chlorination roasting allows certain raw material components to react with a chlorine source to generate volatile chlorides, which can be directly collected by condensation. This method is typically used to recover metals whose chlorination reaction requires a high temperature (e.g., Au, Ag, Pb, and Zn) [10,11]. The moderatetemperature chlorination roasting can reconstruct targeted refractory mineral phases into easily leached phases. The chlorinated product can be treated using a hydrometallurgical process to extract the target metal [12]. The moderate-temperature chlorination roasting is usually used to recover rare metals (e.g., Ni, Co, Li, Ga and Rb) from nickel sulfide ore and electronic waste because the chlorination reaction temperatures of these metals are lower than the boiling points of their metal chlorides [13,14]. Both gaseous (e.g., Cl₂ and HCl) and solid (e.g., CaCl2, MgCl2, NH4Cl, NaCl, and AlCl₃) chlorinating agents are used [15]; however, as gaseous chlorinating agents easily corrode expensive pipelines, solid chlorinating agents are more suitable for the industrial production [16].

In our previous study, the effects of temperature, holding time, the dosage of CaCl₂, roasting atmosphere on the zinc recovery efficiency during high-temperature chlorination volatilization roasting method were investigated [17]. In this study, we explored the mechanism of chlorination roasting through thermodynamic and kinetic analysis. The transformation law of the chloride source was determined by FactSage 7.1 software.

The iron oxidation process during chlorination roasting was investigated by thermal analysis, providing theoretical basis for recovering iron from copper smelting slags. The critical kinetic parameters and mechanism of the Zn recovery process were determined by analyzing the reaction kinetics. Through this study, a new theory and method for resource utilization of copper smelting slag were established.

2 Experimental

2.1 Materials

The copper smelting slag was obtained from a copper smeltery in Shandong Province, China, and the slag was depleted copper by slow-cooling flotation. Analytical reagent CaCl₂·2H₂O was used as the chlorinating agent. Chemical analysis of the copper smelting slag was performed using an inductively coupled plasma-optical spectrometry (ICP-OES, Optima 7300 V, Perkin Elmer), and the results are given in Table 1. The main contents in the copper smelting slag were 2.80% Zn, 45.27% Fe, 35.07% O, and 11.75% Si. The occurrences of Zn and Fe in different phases of the copper smelting slag are given in Table 2 and Table 3, respectively (Detection was carried out in Changsha Research Institute of Mining and Metallurgy, China). The occurrence of Zn in different phases in the copper smelting slag was as

Table 1 Chemical composition of copper smelting slag (wt.%)

Zn	Fe	О	Si	Ca	Na
2.80	45.27	35.07	11.75	1.76	1.36
K	Cu	I	Pb	S	As
0.58	0.55	0	.45	0.41	0.096

Table 2 Occurrence of Zn in different Zn-containing phases in copper smelting slag

Phase	Content/ $(kg \cdot t^{-1})$	Distribution/%
Zn ₂ SiO ₄	13.1	46.74
$ZnFe_2O_4$	9.75	34.79
ZnO	3.15	11.23
ZnS	1.93	6.88
ZnSO ₄	0.1	0.36
Total	28.03	100

Table 3 Occurrence of Fe in different Fe-containing phases in copper smelting slag

Content/ $(kg \cdot t^{-1})$	Distribution/%
242.5	53.57
202.5	44.73
3.1	0.68
2.8	0.62
1.8	0.4
452.7	100
	242.5 202.5 3.1 2.8 1.8

follows: 46.74% Zn₂SiO₄, 34.79% ZnFe₂O₄, 11.23% ZnO, 6.88% ZnS, and 0.36% ZnSO₄. The main Fe-containing phases were Fe₂SiO₄ and Fe₃O₄ with 53.57% and 44.73% of Fe, respectively. The X-ray diffraction (XRD, TTR III, Rigaku) pattern of the copper smelting slag is shown in Fig. 1(a). Fayalite, magnetite, and hedenbergite were the

significant minerals present in the copper smelting slag. Due to the encapsulation of magnetite and fayalite, the minor minerals (e.g., Zn-containing phases) in the copper smelting slag cannot be accurately characterized by XRD. The particle size distribution of the copper smelting slag analyzed by the laser particle size analyzer (Mastersizer 3000, Malvern PANalytical) is shown in Fig. 1(b). The mean diameter of the volume surface, average particle diameter, and specific surface area of the copper smelting slag were 8.368 µm, 30.989 µm, and 717.0 m²/kg, respectively. The scanning electron microscopy-energy dispersive spectroscopy (SEM–EDS, MIRA3, TESCAN) mapping (Fig. 1(c)) showed the distribution of main elements in the copper smelting slag. Further, the mapping results support the occurrence states of Fe, Si, O, and Ca, consistent with the XRD results.

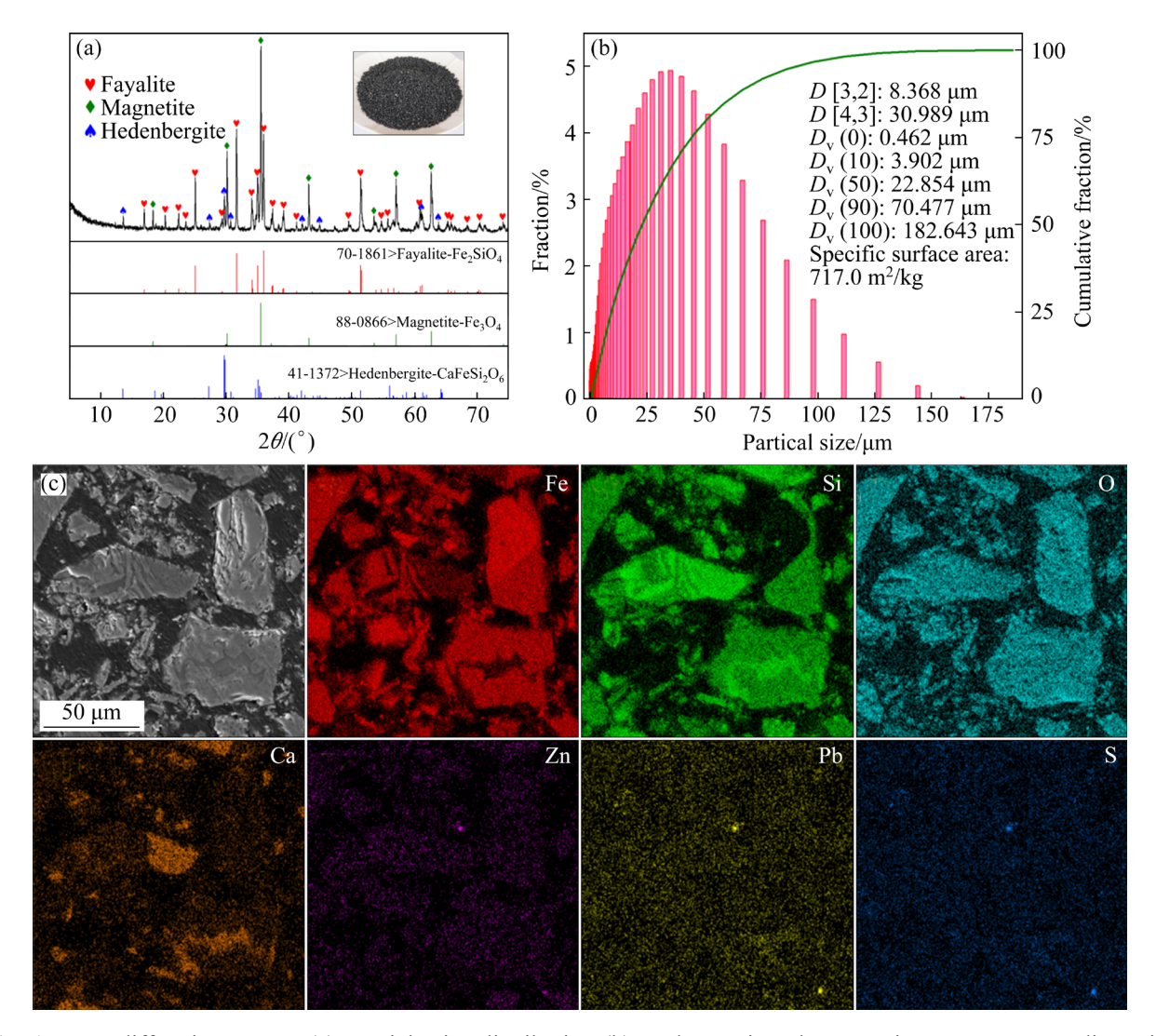


Fig. 1 X-ray diffraction pattern (a), particle size distribution (b), and scanning electron microscopy—energy dispersive spectroscopy mapping (c) of copper smelting slag

2.2 Roasting experiment

All experiments were conducted in a hightemperature stainless-steel tube furnace, as shown in Fig. 2. The 10 g sample of dried copper smelting slag and different amounts of CaCl₂ were mixed and placed in a steel boat. The furnace temperature was increased to the target temperature at a heating rate of 15 °C/min. Subsequently, the steel boat was pushed into the center of the invariable-temperature zone of the furnace by the tongs. Air was introduced at a flow rate of 100 mL/min. Upon completion of roasting, rapid cooling of the sample was achieved by fetching the steel boat outside the furnace using the tongs. Further, the roasted slags were ground into powder and analyzed using ICP-OES and XRD. During the experiment, the volatilized flue gas was gathered through a gas scrubber containing 250 mL of 30% NaOH at the tube furnace outlet. The recovery efficiency of Zn is calculated as

$$R = \frac{w_{\rm g} \cdot m_{\rm g} - w_{\rm s} \cdot m_{\rm s}}{w_{\rm g} \cdot m_{\rm g}} \tag{1}$$

where R is the recovery efficiency (%), w_g is the mass fraction of an element in the copper smelting slag, m_g is the mass of the copper smelting slag in the steel boat, w_s is the mass fraction of an element in the roasting slag, and m_s is the mass of the roasting slag.

2.3 TG-DSC experiment

The thermogravimetry and differential scanning calorimetry (TG–DSC, Diamond 6300, PerkinElmer) analysis was used to investigate the phase transition mechanism and process kinetics during the chlorination roasting. The sample was placed in the analysis instrument in a corundum

crucible and heated from room temperature to $1000\,^{\circ}\text{C}$ in a stable mixed gas atmosphere (20% $O_2 + 80\%\,N_2$) at a $100\,\text{mL/min}$ flow rate under specified heating rate.

3 Results and discussion

3.1 Thermodynamic analysis

To determine the feasibility of recovering Zn from the copper smelting slag by chlorination roasting, the decomposition mechanism CaCl₂·2H₂O in the air was examined using the results of the TG-DSC system at a heating rate of 10 °C/min (Fig. 3). Three stages of mass loss were observed between 30 and 1030 °C. The mass losses of the first stage (30-94 °C) and the second stage (94–160 °C) were 1.99% and 24.76%, respectively, and the corresponding differential scanning calorimetry (DSC) peak values were 47.7 and 178.4 °C. The first and second stages of mass loss were caused by the removal of adsorbed and crystallized water from CaCl₂·2H₂O, respectively. A heat absorption peak of DSC was observed at 774.3 °C; however, there was no mass loss, since the solid CaCl₂ began to melt and turned into liquid CaCl₂. The third stage of mass loss occurred above 774.3 °C, attributed to the evaporation of CaCl₂. These results are consistent with the physicchemical property analysis using alkaline earth metals as chlorinating agents [18,19].

During the roasting process, CaCl₂ can be dissociated to generate Cl₂ or HCl in air atmosphere. The possible dissociation reactions of CaCl₂ in different phases are shown as

$$2CaCl_2+O_2(g)=2Cl_2(g)+2CaO$$
 (2)

$$2CaCl_2+O_2(g)+2SiO_2=2Cl_2(g)+2CaSiO_3$$
 (3)

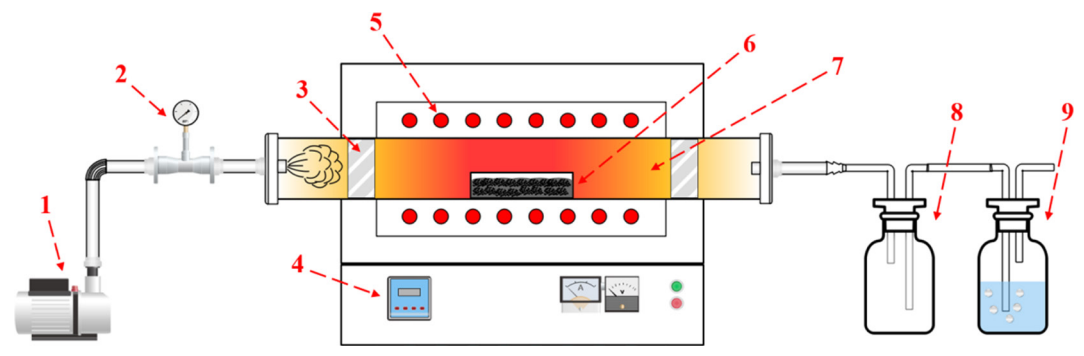


Fig. 2 Experimental setup of chlorination roasting experiment: 1–Air compressor pump; 2–Flowmeter; 3–Insulating brick; 4–Temperature control system; 5–Silicon molybdenum bar; 6–Sample and steel boat; 7–Stainless steel tube; 8–Safety bottle; 9–Absorber bottle containing 30% NaOH

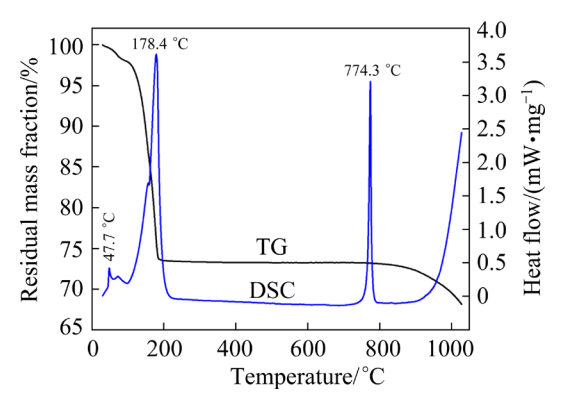


Fig. 3 Thermogravimetry and differential scanning calorimetry curves of CaCl₂·2H₂O in air

$$CaCl2+H2O(g)=CaO+2HCl(g)$$
 (4)

$$CaCl2+H2O(g)+SiO2=CaSiO3+2HCl(g)$$
 (5)

$$2CaCl_2(1)+O_2(g)=2Cl_2(g)+2CaO$$
 (6)

$$2CaCl_2(1)+O_2(g)+2SiO_2=2Cl_2(g)+2CaSiO_3$$
 (7)

$$CaCl2(1)+H2O(g)=CaO+2HCl(g)$$
 (8)

$$CaCl2(1)+H2O(g)+SiO2=CaSiO3+2HCl(g)$$
 (9)

$$2CaCl_2(g)+O_2(g)=2Cl_2(g)+2CaO$$
 (10)

$$2CaCl_2(g)+O_2(g)+2SiO_2=2Cl_2(g)+2CaSiO_3$$
 (11)

$$CaCl2(g)+H2O(g)=CaO+2HCl(g)$$
 (12)

$$CaCl2(g)+H2O(g)+SiO2=CaSiO3+2HCl(g)$$
 (13)

The possible chlorination reactions of each Zn-containing phase in the copper smelting slag can be expressed as

$$Zn_2SiO_4+2Cl_2(g)=2ZnCl_2(g)+SiO_2+O_2(g)$$
 (14)

$$Zn_2SiO_4+4HCl(g)=2ZnCl_2(g)+SiO_2+2H_2O(g)$$
 (15)

$$2ZnFe_2O_4+2Cl_2(g)=2ZnCl_2(g)+2Fe_2O_3+O_2(g)$$
 (16)

$$ZnFe_2O_4+2HCl(g)=ZnCl_2(g)+Fe_2O_3+H_2O(g)$$
 (17)

$$2ZnO+2Cl_2(g)=2ZnCl_2(g)+O_2(g)$$
 (18)

$$ZnO+2HCl(g)=ZnCl2(g)+H2O(g)$$
 (19)

$$ZnS+Cl_2(g)+O_2(g)=ZnCl_2(g)+SO_2(g)$$
 (20)

$$ZnS+2HCl(g)+1.5O_2(g)=$$

$$ZnCl_2(g)+SO_2(g)+H_2O(g)$$
 (21)

$$ZnSO_4+Cl_2(g)=ZnCl_2(g)+SO_2(g)+O_2(g)$$
 (22)

The Gibbs free energy changes (ΔG^{Θ}) of these chemical reactions were calculated by FactSage 7.1 software, and the results are shown in Fig. 4. According to the TG-DSC results of CaCl₂, the

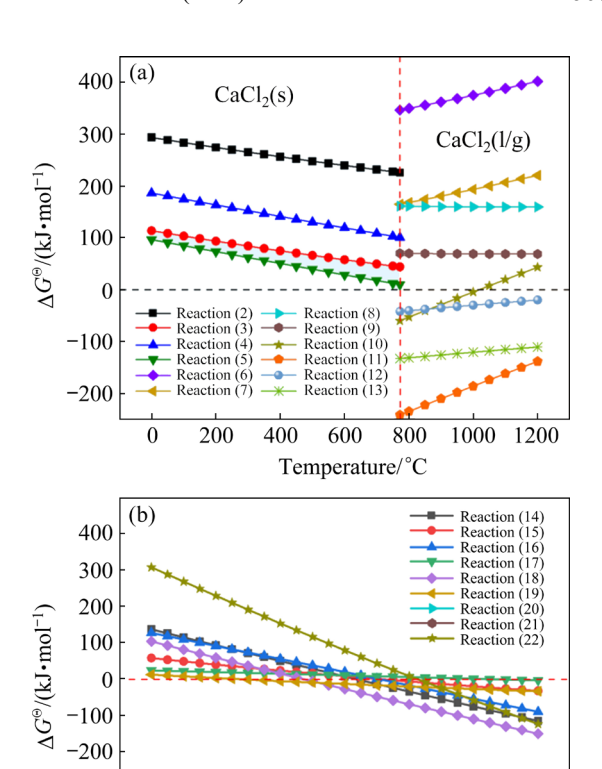


Fig. 4 Gibbs free energy change as function of temperature for chemical reactions during chlorination roasting: (a) CaCl₂; (b) Zn-containing phases

Temperature/°C

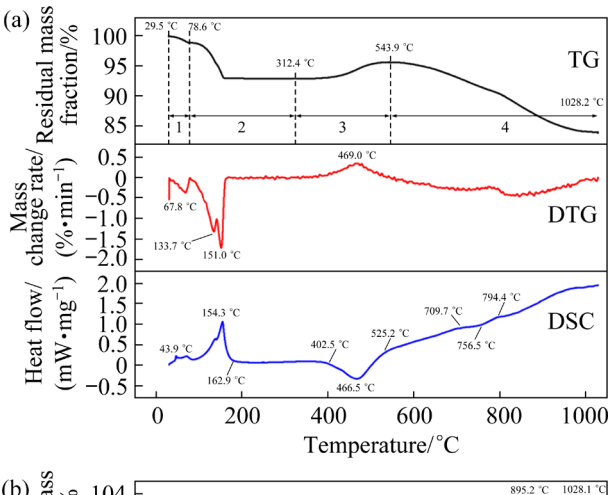
1000

-300 -400

solid CaCl₂ could be melted and gradually volatilized above 774.3 °C. Hence, the calculated temperature of Reactions (2)-(13) was divided into 0-774.3 °C (solid phase) and 774.3-1200 °C (liquid/gas phase), as shown in Fig. 4(a). It is indicated that dissociation reactions of solid and liquid CaCl₂ are difficult to proceed, while the gas CaCl₂ can be easily dissociated to Cl₂ or HCl. The correlation of ΔG^{Θ} with temperature for Reactions (14)–(22) are shown in Fig. 4(b). It could be speculated that all chlorination reactions of ZnS can occur in the temperature range of 0-1200 °C; Zn₂SiO₄ and ZnFe₂O₄ are preferentially chlorinated by Cl₂, and their initial reaction temperatures are 635 and 706 °C, respectively; ZnO is preferentially chlorinated by HCl at temperatures above 264 °C; ZnSO₄ is more difficult to be chlorinated than other Zn-containing phases, and the initial temperature of chlorination reaction with Cl₂ is 825 °C. In general, all zinc-containing phases in the copper smelting slag can be spontaneously chlorinated at temperatures above 825 °C.

3.2 Procedure analysis

The chlorination roasting mechanism (copper smelting slag + 30 wt.% CaCl₂) was determined through the thermogravimetric (TG) analysis, with an airflow rate of 100 mL/min and at a heating rate of 10 °C/min (Fig. 5(a)). The entire chlorination roasting process was divided into four stages. In the first stage, a mass loss of 1.13% was observed over the temperature range of 29.5–78.6 °C, attributed to the precipitation of adsorbed water.



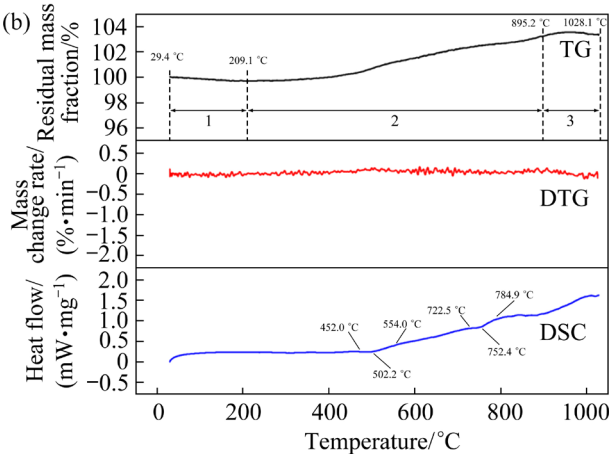


Fig. 5 TG-DTG-DSC curves of copper smelting slag after chlorination roasting: (a) With 30 wt.% CaCl₂; (b) Without CaCl₂

The second stage took place over the temperature range of 78.6–312.4 °C, with a mass loss of 5.98% due to the extraction of crystallized water. The mass losses in the first and second stages were consistent with the DSC heat absorption peaks observed at 43.9 and 154.3 °C, respectively. The derivative thermogravimetric (DTG) analysis showed that the fastest mass loss rate during chlorination roasting occurred in the second stage.

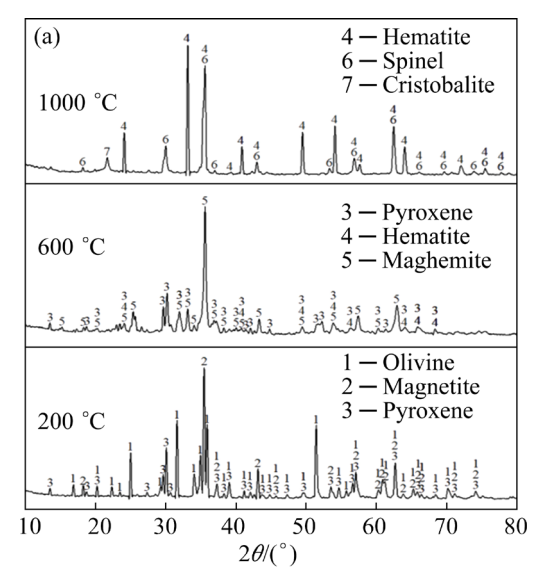
The third stage began at 312.4 °C and ended at

543.9 °C, resulting in a mass gain of 2.75%. DSC analysis showed an exothermic peak at 466.5 °C, indicating that the oxidation of Fe-containing phases (Fe₂SiO₄/Fe₃O₄ \rightarrow Fe₂O₃) occurred in the third stage.

The fourth stage began at 543.9 °C and ended at 1028.2 °C, in which the sample mass was reduced by 11.63%. The DSC curve showed an upward trend with no significant concave or convex peaks, possibly because of the continuous vaporization of CaCl₂ with increasing temperature. The chlorination reaction of Zn was not confirmed by DSC, as there were traces of Zn in the copper smelting slag.

The TG analyses of the roasting of copper smelting slag without CaCl2 in air are shown in Fig. 5(b). Since the DTG curve had no apparent characteristics, the TG and DSC curves were mainly analyzed. The entire blank roasting process was divided into three stages. In the first stage, mass loss of 0.31% was observed over the temperature range of 29.4-209.1 °C, attributed to the removal of adsorbed and crystallized water in the copper smelting slag. In the second stage, the sample mass increased by 3.52% and a DSC concave peak was observed at 452-554 °C, attributed to the oxidation of Fe-containing phases. This result is in good agreement with that of the third stage shown in Fig. 5(a). The temperature range of the third stage was 895.4-1028.1 °C, and the mass loss at this stage was 0.06%. The DSC curve of the third stage showed no obvious changes; therefore, it was concluded that the mass loss was caused by the volatilization of trace substances in the materials.

To further investigate the phase transformation behavior during the roasting of copper smelting slag, contrast tests were performed at different roasting temperatures and with proportioning schemes. The copper smelting slag was roasted at 200, 600, and 1000 °C for 30 min with an airflow rate of 100 mL/min. The XRD patterns are shown in Fig. 6(a). At 200 °C, the main phases in the roasting slag remained unchanged in contrast to that of the raw material (shown in Fig. 1(a)). At 600 °C, hematite and maghemite were the main Fecontaining phases in the roasting slag. When the temperature was increased to 1000 °C, the diffraction peaks of maghemite were no longer detected, and the only remaining Fe-containing



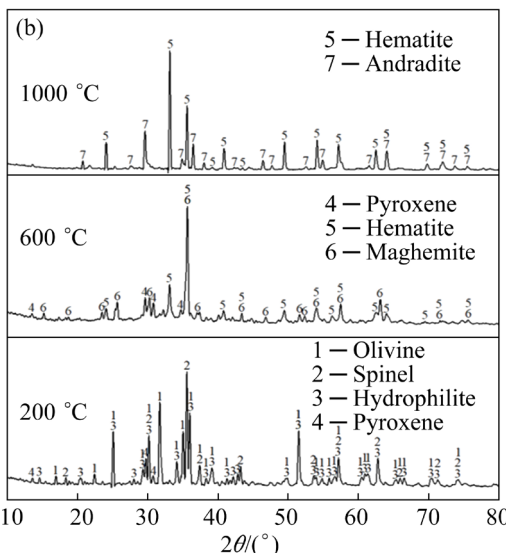


Fig. 6 X-ray diffraction patterns of slags at different roasting temperatures: (a) Copper smelting slag; (b) Copper smelting slag + 30 wt.% CaCl₂

phase was hematite, indicating that Fe was completely oxidized at 1000 °C. Under the same roasting conditions, chlorination roasting was conducted on the copper smelting slag with 30 wt.% CaCl₂. The XRD patterns (Fig. 6(b)) show that the CaCl₂ was dehydrated completely and not decomposed to generate gaseous Cl₂ at 200 °C, given that other chlorides cannot be detected in the XRD pattern and metal chloride cannot be volatilized at low temperatures. When the temperature reached 600 °C, the diffraction peaks of hematite and maghemite appeared and the diffraction peak of chloride disappeared, indicating that Fe in the raw material was oxidized. Meanwhile, the gaseous Cl₂ was produced and

directly volatilized at 600 °C. When the temperature reached 1000 °C, Ca from the chlorination agent reacted with Fe and Si and the diffraction peak of andradite appeared. During this stage, volatile ZnCl₂ was produced by chlorination because the diffraction peak of chloride was not detected at 1000 °C.

3.3 Kinetics analysis of oxidation stage

In this study, the kinetics analysis was used to analyze the roasting process [20]. The activation energy (E) of the Fe oxidation reaction and the kinetic equations were obtained by three methods: Flynn-Wall-Ozawa (FWO), Kissinger, and Coats-Redfern. The non-isothermal DSC curves of the mixture of copper smelting slag and CaCl₂·2H₂O at an airflow rate of 100 mL/min and heating rates of 5, 10, 15, and 20 K/min are presented in Fig. 7(a). The DSC curves exhibited the same trend at different heating rates in the temperature range of 400-540 °C, and the peak area gradually became obvious with increasing heating rate, indicating the Fe oxidation reaction (as shown in Fig. 6(a)). The relationship between the conversion rate and temperature was obtained by integrating the oxidation reaction peak values at different heating rates (Fig. 7(b)). The activation energy of oxidation reaction kinetics was analyzed by FWO and Kissinger methods, and the most probable mechanism function of the iron oxidation was determined by Coats-Redfern method (Fig. 7(b)). The main equations are as follows [21]:

Mass action law:

$$\frac{\mathrm{d}a}{\mathrm{d}t} = k(1-a)^n \tag{23}$$

Arrhenius equation:

$$k = A \exp[E/(RT)] \tag{24}$$

Flynn-Wall-Ozawa method:

$$\lg \beta = \lg \frac{AE}{R(1-a)^n} - 0.4567 \frac{E}{RT} - 2.315$$
 (25)

Kissinger method:

$$\ln \frac{\beta}{T_{\rm p}^{2}} = \ln \frac{AR}{E} - \frac{E}{RT_{\rm p}} \tag{26}$$

Coats-Redfern method:

$$\ln \frac{G(a)}{T^2} = \ln \frac{AR}{\beta E} - \frac{E}{RT} \tag{27}$$

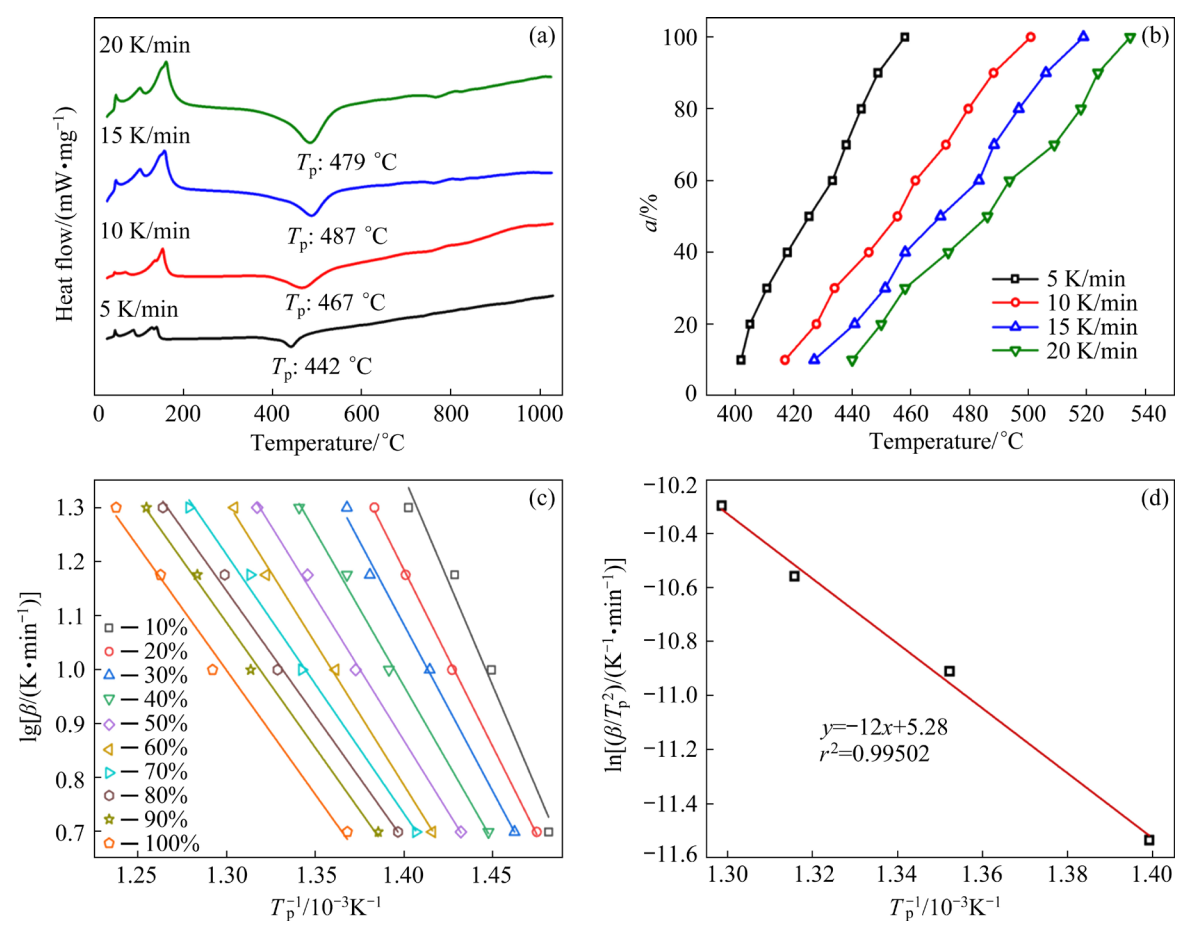


Fig. 7 Differential scanning calorimetry curves of chlorination roasting at different heating rates (a); relationship between conversion rate and temperature at different heating rates (b); relationship between $\lg \beta$ and 1/T at different conversion rates (c); relationship between $\ln(\beta/T_p^2)$ and $1/T_p$ (d)

where α is the conversion rate, %; t is the time, s; k is the reaction rate constant, s⁻¹; n is the reaction order; A is the pre-exponential factor, s⁻¹; E is the apparent activation energy, kJ/mol; E is the molar gas constant, 8.314 J/(mol·K); E is the temperature, K; E is the heating rate, K/min; E is the peak temperature of the DSC curves shown in Fig. 7(a), K; E is the integral form of the kinetic model function given in Table 4 [22].

The relationship between $\lg \beta$ (heating rate) and 1/T of the oxidation reaction under different conversion rates was fitted using the FWO method (Fig. 7(c)). The values of the slopes, coefficient of determination (r^2), and activation energy (E) for different conversion rates are shown in Table 5. The average E value of the oxidation reaction obtained by the FWO method was 102.18 kJ/mol. The relationship between $\lg(\beta/T_p^2)$ and 1/T of the oxidation reaction was fitted using the Kissinger method (Fig. 7(d)), and the kinetic parameters were calculated (Table 6). The E value of the oxidation

reaction obtained by the Kissinger method was 99.77 kJ/mol, which is similar to that calculated by the FWO method. Further, to determine the reaction mechanism model of the oxidation reaction, the Coats-Redfern method was used and the average values of E, A, and r^2 at different heating rates were obtained (Table 7). The average E of 103.16 kJ/mol calculated by Avrami-Erofeev model (A2) was comparable with that calculated by the FWO and Kissinger methods. Therefore, the most probable mechanism function for describing the iron oxidation process was the Avrami-Erofeev model $(G(\alpha)=[-\ln(1-\alpha)]^{1/2})$. The average values of E and $\ln A$ in the oxidation stage calculated by the above methods were 101.7 kJ/mol and 12.03, respectively (Table 8). Hence, the kinetic equation of the oxidation stage during chlorination roasting is expressed as follows:

$$[-\ln(1-a)]^{1/2} = 1.68 \times 10^5 \exp(-\frac{1.02 \times 10^5}{RT})t \qquad (28)$$

 Table 4 Reaction models and corresponding solid

 reaction functions

Symbol	Reaction model	$G(\alpha)$
A1	Avrami–Erofeev (<i>n</i> =1)	$-\ln(1-\alpha)$
A2	Avrami–Erofeev (<i>n</i> =2)	$[-\ln(1-\alpha)]^{1/2}$
D1	One-dimensional diffusion	α^2
D2	Two-dimensional diffusion	$\alpha + (1-\alpha)\ln(1-\alpha)$
P2	Power law $(n=2)$	$lpha^{1/2}$
P3	Power law $(n=3)$	$lpha^{1/3}$
R1	Phase boundary reaction (<i>n</i> =1)	α
R2	Phase boundary reaction (<i>n</i> =2)	$1-(1-\alpha)^{1/2}$

Table 5 Parameters calculated by Flynn–Wall–Ozawa method

memou			
a/%	Slope	$E/(kJ \cdot mol^{-1})$	r^2
10	-7.74	142.62	0.97902
20	-6.55	120.72	0.99938
30	-6.17	113.72	0.99468
40	-5.74	105.70	0.9957
50	-5.32	97.97	0.99726
60	-5.27	97.09	0.99698
70	-4.80	88.49	0.99505
80	-4.63	85.25	0.99549
90	-4.46	82.48	0.99602
100	-4.60	84.77	0.99169
Average	·	102.18	

Table 6 Kinetic parameters calculated by Kissinger method

Slope	Intercept	$E/(kJ \cdot mol^{-1})$	$ln(A/s^{-1})$	r^2
-12.01	5.28	99.77	7.77	0.99502

Table 7 Average model fitting data at different heating rates calculated by Coats–Redfern method

Model -	Kine	tic parameter	
Model	$E/(kJ \cdot mol^{-1})$	$ln(A/s^{-1})$	r^2
A1	217.91	36.57	0.95224
A2	103.16	16.28	0.94691
D1	284.37	46.97	0.88496
D2	350.04	58.09	0.91688
P2	62.35	6.23	0.85470
Р3	37.68	2.39	0.82803
R1	136.36	21.62	0.87595
R2	176.33	28.28	0.94102

Table 8 Activation energy (E) and frequency factor $(\ln A)$ of oxidation reaction calculated by different methods and their average values

M 4 1	Kinetic parameter		
Method	$E/(kJ \cdot mol^{-1})$	$ln(A/s^{-1})$	
Flynn–Wall–Ozawa	102.18	_	
Kissinger	99.77	7.77	
Coats-Redfern	103.16	16.28	
Average	101.70	12.03	

3.4 Reaction kinetics of chlorination stage

3.4.1 Effects of roasting temperature and time

The effects of roasting temperature and time on the recovery efficiency of Zn were studied, with 30 wt.% of CaCl₂ at an airflow rate of 100 mL/min. The recovery efficiency of Zn increased with increasing roasting temperature and holding time (Fig. 8), due to the destruction of copper smelting slag frame at high temperatures, which enhanced the mass transfer process of chlorination [17]. The recovery efficiency of Zn was 97.99% at a roasting temperature of 1000 °C with a roasting time of 16 min. At roasting temperatures of 800, 850, 900, and 950 °C, the chlorination almost reached equilibrium in 30, 30, 20, and 20 min, respectively.

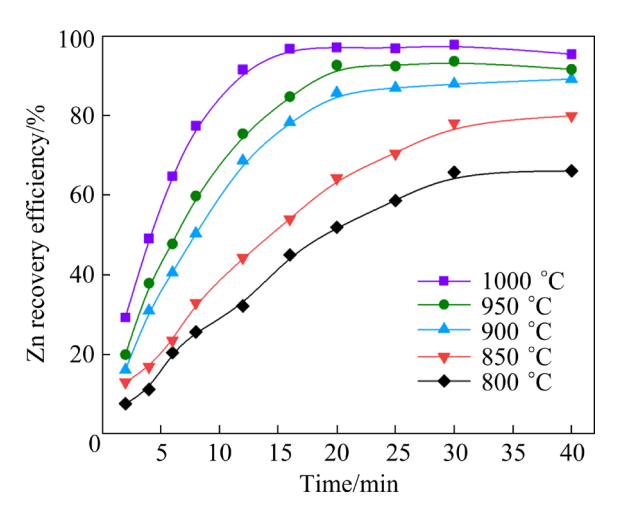


Fig. 8 Effects of roasting temperature on Zn recovery efficiency

3.4.2 Determination of chlorination kinetic model

It is assumed that the Zn-containing phases in the copper smelting slag are dense solid particles with identical chemical activities on their surfaces. The chlorination reaction can be divided into five consecutive steps as follows:

- (1) Mass transfer step: Gaseous CaCl₂ reacted with O₂ and H₂O in the air to form Cl₂ and HCl, which diffused to the surface of the Zn-containing phases in the copper smelting slag.
- (2) Internal diffusion step: Under the action of molecular force field, the Zn-containing phases in the copper smelting slag adsorbed Cl₂ and HCl.
- (3) Chemical reaction step: Gaseous ZnCl₂ was generated during chlorination roasting on the surface of the Zn-containing phases.
- (4) External diffusion step: Gaseous ZnCl₂ diffused into the gas film through the product layer.
- (5) Mass transfer step II: Gaseous $ZnCl_2$ diffused into the air from the gas film.

The shrinking unreacted core model can be used to analyze the chlorination kinetic model because the reactant particles gradually shrink during chlorination [23]. Several studies [24,25] have demonstrated that the mass transfer is not the rate-controlling step during chlorination roasting. In this study, the rate-controlling step may be chemical reaction, external diffusion, or internal diffusion [26]. The kinetic equations of chemical

reaction control, external diffusion control, and internal diffusion control in the shrinking unreacted core model can be expressed as Eqs. (29), (30), and (31), respectively:

$$1 - (1 - a')^{1/3} = kt (29)$$

$$1 - (1 - a')^{2/3} = kt \tag{30}$$

$$1+2(1-a')-3(1-a')^{2/3}=kt$$
(31)

where a' represents the recovery efficiency of Zn, %.

The fitting results of the kinetic equations as functions of time are shown in Figs. 9(a-c). The coefficient of determination (r^2) can be used to determine the goodness of fit of the regression line to the observed value [27]. The fit can be considered good when r^2 approaches 1. $F_1(a')$ provided excellent straight-line fits (the average r^2 of 0.987) for Zn recovery from copper smelting slags, indicating that the chlorination reaction rate was controlled by the chemical reaction (Fig. 9(a)). The relationship between $\ln k$ and 1/T of the chlorination reaction was fitted using the Arrhenius

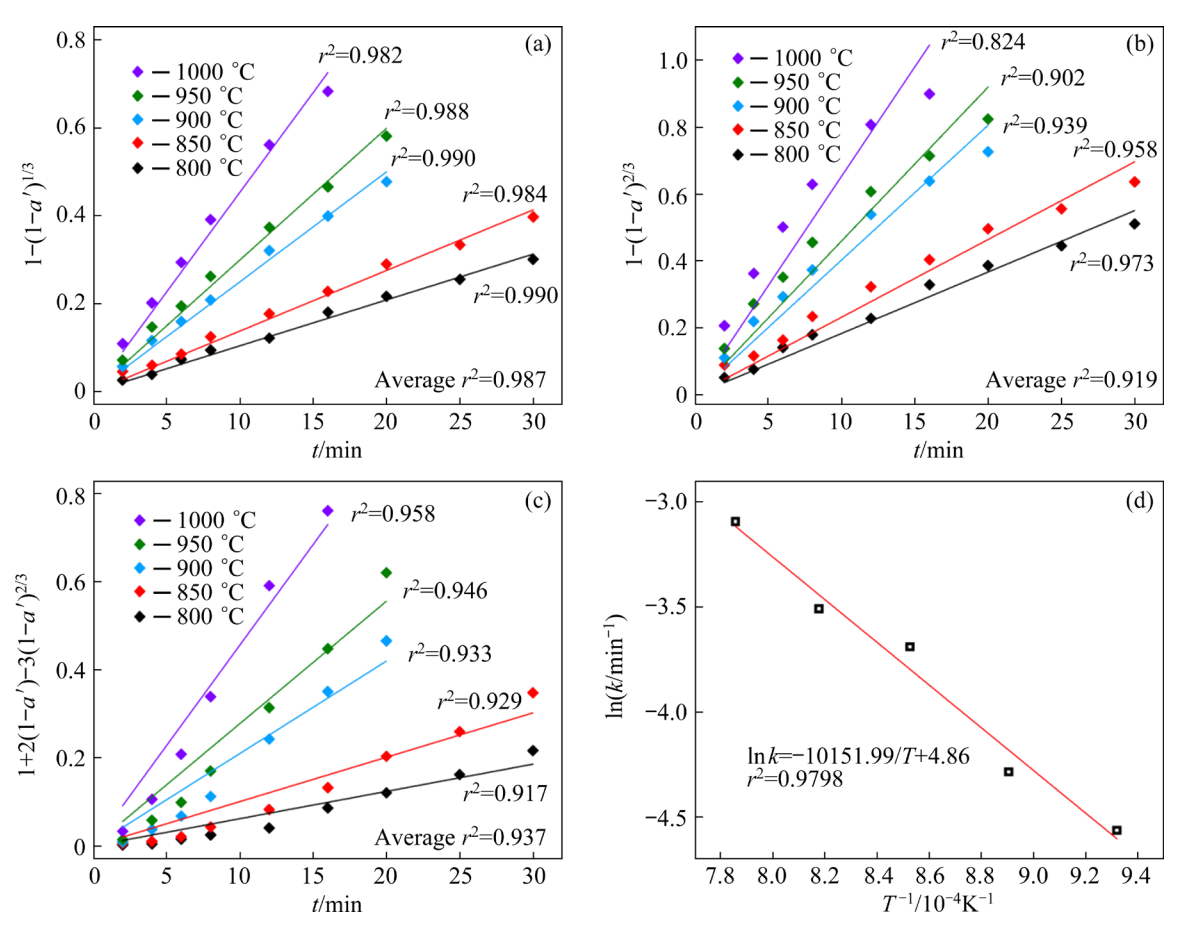


Fig. 9 Relationship between kinetic equations (F(a')) and time (t) at different temperatures: (a) $F_1(a')=1-(1-a')^{1/3}$; (b) $F_2(a')=1-(1-a')^{2/3}$; (c) $F_3(a')=1+2(1-a')-3(1-a')^{2/3}$; (d) Relationship between $\ln k$ and 1/T

equation, as shown in Fig. 9(d). The values of E and r^2 of the chlorination reaction were 84.4 kJ/mol and 0.9798, respectively. Notably, the reaction process was controlled by the chemical reaction when the apparent activation energy was greater than 40 kJ/mol, thus confirming the significance of rate-determining step in the chlorination reaction [28]. The intercept of the fitted straight line in Fig. 9(d) was used to obtain the pre-exponential factor (A=128.85 s⁻¹).

3.5 Behavior of other elements during chlorination roasting process

A copper smelting slag of 10 g, CaCl₂ dosage of 30%, airflow rate of 100 mL/min, and roasting time of 16 min were used to study the influence of roasting temperature on the volatilization efficiencies of Pb, Cu, Fe, Si, S, and As in the copper smelting slag. The results are shown in Fig. 10. Fe was difficult to be evaporated from the copper smelting slag and retained in the roasting slag, even when the roasting temperature was as high as 1000 °C. The volatilization efficiency of As did not change significantly during the roasting process 800-1000 °C. The volatilization efficiency of Si decreased slowly as the temperature increased. The volatilization efficiency of Pb increased significantly with increasing temperature and reached 99.81% at 1000 °C. This is because the Pb-containing phases in the copper smelting slag were easily chlorinated and produced gaseous PbCl₂ at high temperatures [17]. The volatilization efficiency of S also increased significantly with increasing temperature, attributed to the thermal decomposition of sulfate [11]. Further, the recovery efficiency of Cu is noteworthy because 0.55 wt.% copper in the copper smelting slag has considerable recovery value. The volatilization efficiency of Cu increased slowly with increasing temperature (800–1000 °C); however, the highest volatilization efficiency was only 27.06%. Typically, Cucontaining phases in the copper smelting slag are easily chlorinated with chlorine sources (e.g., Cl₂ and HCl) and produce volatile CuCl [29]. However, Cu₂O is formed through the reaction of CuCl and surplus O₂, thereby reducing the volatilization efficiency of Cu. Here, it is demonstrated that the high-temperature chlorination roasting can selectively recover the target metal from copper smelting slag, and the effective recovery of Cu from the roasting slag will be investigated in future research

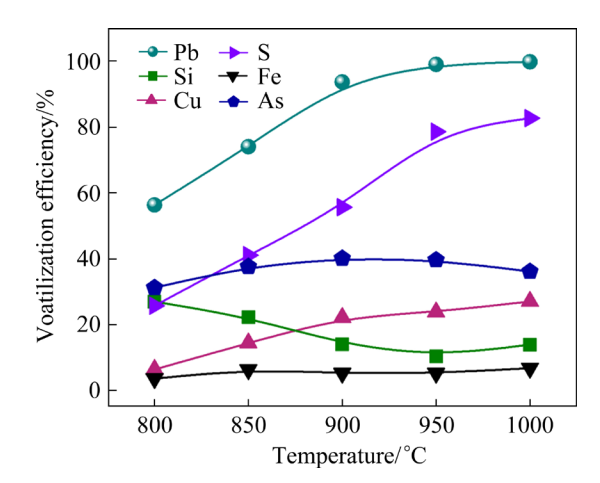


Fig. 10 Behavior of other elements in chlorination roasting process

4 Conclusions

- (1) The TG-DSC and thermodynamics analyses indicated that CaCl₂ can provide Cl₂ and HCl to the chlorination reaction at temperatures above 774.3 °C. All Zn-containing phases in the copper smelting slag can be chlorinated by Cl₂ and HCl at temperatures above 825 °C.
- (2) The TG-DSC analysis of the mixed materials indicated that the entire chlorination roasting process was mainly divided into four stages: precipitation of adsorbed water, extraction of crystallized water, oxidation of Fe-containing phases, and chlorination reaction of Zn.
- (3) The kinetics analysis revealed that the E value of the iron oxidation reaction during chlorination roasting was 101.70 kJ/mol and $\ln A$ was 12.03. The most probable mechanism function for describing the iron oxidation process was $G(\alpha) = [-\ln(1-\alpha)]^{1/2}$. The kinetic equation for the iron oxidation reaction is $[-\ln(1-a)]^{1/2} = 1.68 \times 10^5 \cdot \exp[-1.02 \times 10^5/(RT)]t$.
- (4) Investigation of the reaction kinetics of zinc during chlorination roasting showed that the zinc chlorination process followed the shrinking unreacted core model, and the chemical reaction was the rate-controlling step. The apparent activation energy of the zinc chlorination process was 84.4 kJ/mol.

Acknowledgments

The authors gratefully acknowledge the

financial support from the National Natural Science Foundation of China (Nos. 51904351, 51620105013 and U20A20273), the Innovation-Driven Project of Central South University, China (No. 2020CX028), the Natural Science Fund for Distinguished Young Scholar of Hunan Province, China (No. 2019JJ20031), and the National Key R&D Program of China (Nos. 2018YFC1902500 and 2019YFC1907400).

References

- [1] HAWKER W, VAUGHAN J, JAK E, HAYES P C. The synergistic copper process concept [J]. Mineral Processing and Extractive Metallurgy, 2018, 127(4): 210–220.
- [2] ZHANG H B, HE Y Z, HU J J, WANG Y N, CAO H Z, ZHOU J, ZHENG G Q. Assessment of selective sequential extraction procedure for determining arsenic partitioning in copper slag [J]. Transactions of Nonferrous Metals Society of China, 2020, 30(10): 2823–2835.
- [3] TURAN M D, SARI Z A, MILLER J D. Leaching of blended copper slag in microwave oven [J]. Transactions of Nonferrous Metals Society of China, 2017, 27(6): 1404–1410.
- [4] TIAN H Y, GUO Z Q, PAN J, ZHU D Q, YANG C C, XUE Y X, LI S W, WANG D Z. Comprehensive review on metallurgical recycling and cleaning of copper slag [J]. Resources, Conservation and Recycling, 2021, 168: 105366.
- [5] TSUNAZAWA Y, LIU C Z, TOI R, OKURA T, TOKORO C. Crystal formation and growth by slow cooling for recovery of magnetite particles from copper smelting slag [J]. Mineral Processing and Extractive Metallurgy, 2019, 128(4): 248–255.
- [6] ZHANG S H, ZHU N W, MAO F L, ZHANG J Y, HUANG X X, LI F, LI X Y, WU P X, DANG Z. A novel strategy for harmlessness and reduction of copper smelting slags by alkali disaggregation of fayalite (Fe₂SiO₄) coupling with acid leaching [J]. Journal of Hazardous Materials, 2021, 402: 123791.
- [7] WAN X B, TASKINEN P, SHI J J, JOKILAAKSO A. A potential industrial waste-waste co-treatment process of utilizing waste SO₂ gas and residue heat to recover Co, Ni, and Cu from copper smelting slag [J]. Journal of Hazardous Materials, 2021, 414: 125541.
- [8] ZULHAN Z, FAUZIAN I M, HIDAYAT T. Ferro-silicomanganese production from manganese ore and copper smelting slag [J]. Journal of Materials Research and Technology, 2020, 9(6): 13625–13634.
- [9] JENA P K, BROCCHI E A. Metal extraction through chlorine metallurgy [J]. Mineral Processing and Extractive Metallurgy Review, 1997, 16(4): 211–237.
- [10] LI H Y, PENG J H, MA P C, ZHOU Z F, LONG H L, LI S W, ZHANG L B. Application of diagnostic roasting method in thermochemical treatment for Au recovery from gold-containing tailings in microwave field [J]. Minerals Engineering, 2021, 163: 106773.
- [11] QIN H, GUO X Y, TIAN Q H, ZHANG L. Pyrite enhanced

- chlorination roasting and its efficacy in gold and silver recovery from gold tailing [J]. Separation and Purification Technology, 2020, 250: 117168.
- [12] MU W N, CUI F H, XIN H X, ZHAI Y C, XU Q. A novel process for simultaneously extracting Ni and Cu from mixed oxide—sulfide copper—nickel ore with highly alkaline gangue via FeCl₃·6H₂O chlorination and water leaching [J]. Hydrometallurgy, 2020, 191: 105187.
- [13] XIAO J F, GAO R T, NIU B, XU Z M. Study of reaction characteristics and controlling mechanism of chlorinating conversion of cathode materials from spent lithium-ion batteries [J]. Journal of Hazardous Materials, 2021, 407: 124704.
- [14] CUI F H, MU W N, ZHAI Y C, GUO X Y. The selective chlorination of nickel and copper from low-grade nickel-copper sulfide-oxide ore: Mechanism and kinetics [J]. Separation and Purification Technology, 2020, 239: 116577.
- [15] MUKHERJEE T K, GUPTA C K. Base metal resource processing by chlorination [J]. Mineral Processing and Extractive Metallurgy Review, 1983, 1(1/2): 111–153.
- [16] LI L, HU J H, WANG H. Application of the chloridizing roasting method for the removal of copper and sulphur from copper slags [J]. Mineral Processing and Extractive Metallurgy, 2018, 127(1): 49–55.
- [17] GUO X Y, ZHANG B K, WANG Q M, LI Z C, TIAN Q H. Recovery of zinc and lead from copper smelting slags by chlorination roasting [J]. JOM, 2021, 73(6): 1861–1870.
- [18] LI H Y, PENG J H, LONG H L, LI S W, ZHANG L B. Cleaner process: Efficacy of chlorine in the recycling of gold from gold-containing tailings [J]. Journal of Cleaner Production, 2021, 287: 125066.
- [19] LI H Y, LI S W, MA P C, ZHOU Z F, LONG H L, PENG J H, ZHANG L B. Evaluation of a cleaner production for cyanide tailings by chlorination thermal treatments [J]. Journal of Cleaner Production, 2021, 281: 124195.
- [20] MU W N, CHENG H, XU J, LUO S H, ZHAI Y C, XU Q. Extraction of valuable metals from low-grade nickel matte by FeCl₃·6H₂O roasting and water leaching process with studies on phase evolution and kinetics analysis of chlorination process [J]. Hydrometallurgy, 2021, 202: 105614.
- [21] OUYANG Z, LIU S F, TANG C B, CHEN Y F, YE L G. Kinetic studies for sulfur-fixing and roasting reduction of antimony sulfide for direct antimony extraction [J]. Vacuum, 2019, 159: 358–366.
- [22] OUYANG Z, CHEN Y F, TIAN S Y, XIAO L, TANG C B, HU Y J, XIA Z M, CHEN Y, YE L G. Thermodynamic and kinetics analysis of the sulfur-fixed roasting of antimony sulfide using ZnO as sulfur-fixing agent [J]. Journal of Mining and Metallurgy Section B: Metallurgy, 2018, 54: 31.
- [23] LU C Y, ZOU X L, LU X G, XIE X L, ZHENG K, XIAO W, CHENG H W, LI G S. Reductive kinetics of Panzhihua ilmenite with hydrogen [J]. Transactions of Nonferrous Metals Society of China, 2016, 26(12): 3266–3273.
- [24] LEI C, CHEN T, YAN B, XIAO X M. Reaction characteristics and kinetics of gallium in chlorination roasting of copper tailings using calcium chloride [J]. Rare Metals, 2022, 41(3): 1063–1070.

- [25] SUI L L, ZHAI Y C. Reaction kinetics of roasting high-titanium slag with concentrated sulfuric acid [J]. Transactions of Nonferrous Metals Society of China, 2014, 24(3): 848–853.
- [26] GONG D D, ZHOU K G, LI J J, PENG C H, CHEN W. Kinetics of roasting reaction between synthetic scheelite and magnesium chloride [J]. JOM, 2019, 71(8): 2827–2833.
- [27] FOUGA G G, PASQUEVICH D M, BOHÉ A E. The kinetics and mechanism of selective iron chlorination of an
- ilmenite ore [J]. Mineral Processing and Extractive Metallurgy, 2007, 116(4): 230–238.
- [28] CHEN Y L, HUO G S, GUO X Y, WANG Q M. Wolframite concentrate conversion kinetics and mechanism in hydrochloric acid [J]. Minerals Engineering, 2022, 179: 107422.
- [29] LI L, WANG H, HU J H. Smelting chlorination method applied to removal of copper from copper slags [J]. Journal of Central South University, 2015, 22(1): 59–65.

氯化焙烧铜熔炼渣的过程机理及动力学

张倍恺1,2, 王亲猛1,2, 郭学益1,2, 田庆华1,2

- 1. 中南大学 冶金与环境学院,长沙 410083;
- 2. 有色金属资源循环利用国家地方联合工程研究中心,长沙 410083

摘 要:提出一种以 $CaCl_2$ 为氯化剂,采用氯化焙烧法从铜熔炼渣中高效回收锌的工艺。利用热力学计算、热重— 差热(TG-DSC)分析和 X 射线衍射(XRD)等手段,研究氯化反应机理和氯化焙烧过程动力学。结果表明, $CaCl_2$ 氧化分解和所有含锌相的氯化反应温度均分别高于 774.3 和 825 $\mathbb C$ 。铜熔炼渣的氯化焙烧过程可分为 4 个阶段,依次为吸附水脱除、结晶水脱除、含铁相氧化和锌的氯化挥发。铁氧化阶段和锌氯化挥发阶段的表观活化能分别为 101.70 和 84.4 kJ/mol,铁氧化过程的最概然机理函数为 Avrami-Erofeev 方程(n=2),锌氯化过程符合未反应核收缩模型且受化学反应控制。

关键词:铜熔炼渣;氯化焙烧; CaCl2; 热力学; 动力学; 铁; 锌

(Edited by Bing YANG)